Moments of the electron energy spectrum and partial branching fraction of $B \to X_c e \nu$ decays at the Belle detector

P. Urquijo,[22] E. Barberio,[22] K. Abe,[8] K. Abe,[45] I. Adachi,[8] H. Aihara,[47] D. Anipko,[1] V. Aulchenko,[1] T. Aushev,[14,19]
M. Barbero,[7] K. Belous,[13] U. Bitenc,[15] I. Bizjak,[15] S. Blyth,[25] A. Bondar,[1] A. Bozek,[28] M. Bračko,[8,15,21] J. Brodzicka,[28]
T. E. Browder,[7] P. Chang,[27] Y. Chao,[27] A. Chen,[25] K.-F. Chen,[27] W. T. Chen,[25] B. G. Cheon,[3] R. Chistov,[14] Y. Choi,[41]
Y. K. Choi,[41] A. Chuvikov,[36] S. Cole,[42] J. Dalseno,[22] M. Danilov,[14] M. Dash,[51] J. Dragic,[8] A. Drutskoy,[4] S. Eidelman,[1]
S. Fratina,[15] N. Gabyshev,[1] T. Gershon,[8] A. Go,[25] G. Gokhroo,[43] P. Goldenzweig,[4] B. Golob,[15,20] H. Ha,[17] J. Haba,[8]
T. Hara,[33] N. C. Hastings,[47] K. Hayasaka,[23] H. Hayashii,[24] M. Hazumi,[8] D. Heffernan,[33] Y. Hoshi,[45] S. Hou,[25]
W.-S. Hou,[27] T. Iijima,[23] A. Imoto,[24] K. Inami,[23] A. Ishikawa,[47] R. Itoh,[8] M. Iwasaki,[47] Y. Iwasaki,[8] J. H. Kang,[52]
N. Katayama,[8] H. Kawai,[2] T. Kawasaki,[30] H. R. Khan,[48] H. Kichimi,[8] S. K. Kim,[39] Y. J. Kim,[6] K. Kinoshita,[4]
S. Korpar,[15,21] P. Križan,[15,20] P. Krokovny,[8] R. Kulasiri,[4] R. Kumar,[34] C. C. Kuo,[25] A. Kuzmin,[1] Y.-J. Kwon,[52] J. S. Lange,[5]
G. Leder,[12] J. Lee,[39] M. J. Lee,[39] T. Lesiak,[28] J. Li,[7] A. Limosani,[8] S.-W. Lin,[27] D. Liventsev,[14] G. Majumder,[43]
T. Matsumoto,[49] A. Matyja,[28] S. McOnie,[42] W. Mitaroff,[12] K. Miyabayashi,[24] H. Miyake,[33] H. Miyata,[30] Y. Miyazaki,[23]
R. Mizuk,[14] G. R. Moloney,[22] T. Nagamine,[46] Y. Nagasaka,[9] I. Nakamura,[8] E. Nakano,[32] M. Nakao,[8] Z. Natkaniec,[28]
S. Nishida,[8] O. Nitoh,[50] T. Nozaki,[8] S. Ogawa,[44] T. Ohshima,[23] S. Okuno,[16] Y. Onuki,[37] P. Pakhlov,[14] G. Pakhlova,[14]
H. Park,[18] K. S. Park,[41] R. Pestotnik,[15] L. E. Piilonen,[51] Y. Sakai,[8] N. Satoyama,[40] T. Schietinger,[19] O. Schneider,[19]
C. Schwanda,[12] R. Seidl,[10,37] K. Senyo,[23] M. E. Sevior,[22] M. Shapkin,[13] H. Shibuya,[44] B. Shwartz,[1] J. B. Singh,[34]
A. Sokolov,[13] A. Somov,[4] S. Stanič,[31] M. Starič,[15] H. Stoeck,[42] K. Sumisawa,[8] T. Sumiyoshi,[49] S. Y. Suzuki,[8] F. Takasaki,[8]
K. Tamai,[8] N. Tamura,[30] M. Tanaka,[8] G. N. Taylor,[22] Y. Teramoto,[32] X. C. Tian,[35] K. Trabelsi,[7] T. Tsukamoto,[8] S. Uehara,[8]
T. Uglov,[14] K. Ueno,[27] Y. Unno,[3] S. Uno,[8] Y. Usov,[1] G. Varner,[7] K. E. Varvell,[42] S. Villa,[19] C. C. Wang,[27] C. H. Wang,[26]
Y. Watanabe,[48] R. Wedd,[22] E. Won,[17] Q. L. Xie,[11] B. D. Yabsley,[42] A. Yamaguchi,[46] Y. Yamashita,[29] M. Yamauchi,[8]
Y. Yusa,[51] L. M. Zhang,[38] Z. P. Zhang,[38] V. Zhilich,[1] and A. Zupanc[15]

(Belle Collaboration)

[1]*Budker Institute of Nuclear Physics, Novosibirsk*
[2]*Chiba University, Chiba*
[3]*Chonnam National University, Kwangju*
[4]*University of Cincinnati, Cincinnati, Ohio 45221*
[5]*University of Frankfurt, Frankfurt*
[6]*The Graduate University for Advanced Studies, Hayama, Japan*
[7]*University of Hawaii, Honolulu, Hawaii 96822*
[8]*High Energy Accelerator Research Organization (KEK), Tsukuba*
[9]*Hiroshima Institute of Technology, Hiroshima*
[10]*University of Illinois at Urbana-Champaign, Urbana, Illinois 61801*
[11]*Institute of High Energy Physics, Chinese Academy of Sciences, Beijing*
[12]*Institute of High Energy Physics, Vienna*
[13]*Institute of High Energy Physics, Protvino*
[14]*Institute for Theoretical and Experimental Physics, Moscow*
[15]*J. Stefan Institute, Ljubljana*
[16]*Kanagawa University, Yokohama*
[17]*Korea University, Seoul*
[18]*Kyungpook National University, Taegu*
[19]*Swiss Federal Institute of Technology of Lausanne, EPFL, Lausanne*
[20]*University of Ljubljana, Ljubljana*
[21]*University of Maribor, Maribor*
[22]*University of Melbourne, Victoria*
[23]*Nagoya University, Nagoya*
[24]*Nara Women's University, Nara*
[25]*National Central University, Chung-li*
[26]*National United University, Miao Li*
[27]*Department of Physics, National Taiwan University, Taipei*
[28]*H. Niewodniczanski Institute of Nuclear Physics, Krakow*
[29]*Nippon Dental University, Niigata*
[30]*Niigata University, Niigata*

[31]*University of Nova Gorica, Nova Gorica*
[32]*Osaka City University, Osaka*
[33]*Osaka University, Osaka*
[34]*Panjab University, Chandigarh*
[35]*Peking University, Beijing*
[36]*Princeton University, Princeton, New Jersey 08544*
[37]*RIKEN BNL Research Center, Upton, New York 11973*
[38]*University of Science and Technology of China, Hefei*
[39]*Seoul National University, Seoul*
[40]*Shinshu University, Nagano*
[41]*Sungkyunkwan University, Suwon*
[42]*University of Sydney, Sydney NSW*
[43]*Tata Institute of Fundamental Research, Bombay*
[44]*Toho University, Funabashi*
[45]*Tohoku Gakuin University, Tagajo*
[46]*Tohoku University, Sendai*
[47]*Department of Physics, University of Tokyo, Tokyo*
[48]*Tokyo Institute of Technology, Tokyo*
[49]*Tokyo Metropolitan University, Tokyo*
[50]*Tokyo University of Agriculture and Technology, Tokyo*
[51]*Virginia Polytechnic Institute and State University, Blacksburg, Virginia 24061*
[52]*Yonsei University, Seoul*

We report a measurement of the inclusive electron energy spectrum for charmed semileptonic decays of B mesons in a 140 fb^{-1} data sample collected at the $\Upsilon(4S)$ resonance with the Belle detector at the KEKB asymmetric energy e^+e^- collider. We determine the first four moments of the electron energy spectrum for threshold values of the electron energy between 0.4 and 2.0 GeV. In addition, we provide values of the partial branching fraction (zeroth moment) for the same electron threshold energies, and independent measurements of the B^+ and B^0 partial branching fractions at 0.4 GeV and 0.6 GeV electron threshold energies. We measure the independent B^+ and B^0 partial branching fractions with electron threshold energies of 0.4 GeV to be $\Delta\mathcal{B}(B^+ \rightarrow X_c e\nu) = (10.79 \pm 0.25(\text{stat.}) \pm 0.27(\text{sys.}))\%$ and $\Delta\mathcal{B}(B^0 \rightarrow X_c e\nu) = (10.08 \pm 0.30(\text{stat.}) \pm 0.22(\text{sys.}))\%$. Full correlations between all measurements are evaluated.

I. INTRODUCTION

The Cabibbo-Kobayashi-Maskawa (CKM) matrix element V_{cb}—the coupling of the b quark to the c quark—is a fundamental parameter of the standard model. The magnitude of V_{cb} can be extracted from the inclusive decay rate of charmed semileptonic B-meson decays $\mathcal{B}(B \rightarrow X_c \ell \nu)$ [1,2]. This paper focuses on measurements to improve the extraction of the quark mixing parameter $|V_{cb}|$, and parameters related to the mass and kinetic energy of the b-quark inside the B meson, m_b or $\bar{\Lambda}$, and μ_π or λ_1 respectively, from the inclusive decay spectra of charmed semileptonic B meson decays.

Several studies have shown that the spectator model decay rate, in which bound state effects are neglected, is the leading term in a well-defined expansion controlled by the parameter Λ_{QCD}/m_b [3–5]. Nonperturbative corrections to this leading approximation arise only to order $1/m_b^2$. The key issue in this approach is the ability to separate nonperturbative corrections (expressed as a series in powers of $1/m_b$), and perturbative corrections (expressed in powers of α_s). There are various different

methods to handle the energy scale μ used to separate long-distance from short-distance physics.

The coefficients of the $1/m_b$ power terms are expectation values of operators that include nonperturbative physics. In this framework, nonperturbative corrections are parametrized by quark masses and matrix elements of higher dimensional operators which are presently poorly known. The experimental accuracy already achieved, and that expected from larger data sets recorded by the B-factories, make the ensuing theory uncertainty a major limiting factor. The extraction of the nonperturbative parameters describing the heavy quark masses, kinetic energy of the b quark and the $1/m_b^3$ corrections directly from the data has therefore become a key issue.

The shapes of the lepton energy spectrum and hadronic mass spectrum provide constraints on the heavy quark expansion (HQE) [6] based on local Operator Product Expansion (OPE) [7]. The noncalculable, nonperturbative quantities are parametrized in terms of expectation values of hadronic matrix elements, which can be related to the shape (characterized by moments) of inclusive decay spectra [8,9]. Measurements of moments to high order with

maximum possible phase space coverage may uncover inconsistencies in the theory. So far, measurements of the electron energy distribution have been made by the DELPHI, CLEO, BaBar and Belle collaborations [10–13].

The hadronic mass moments have high sensitivity to the leading order terms of the OPE. The shape of the lepton spectrum, which is determined with greater experimental precision, is not only sensitive to leading order terms but can also constrain higher order $1/m_b$ corrections, which are the limiting factor on the precision of the theory.

In this paper we report a measurement of the first four moments of the electron energy spectrum and the partial inclusive branching fractions with minimum electron energy thresholds ranging between 0.4 and 2.0 GeV in the B meson rest frame. We also provide separate measurements of $\Delta\mathcal{B}(B^+ \to X_c e\nu)$ and $\Delta\mathcal{B}(B^0 \to X_c e\nu)$[14] for electron energy thresholds of 0.4 GeV and 0.6 GeV. The measurements of these independent partial branching fractions at 0.6 GeV supersede and improve upon previous results reported by the Belle Collaboration [15], and are the most precise measurements to date, while the measurement at 0.4 GeV sets a new lower limit of such a measurement at a B factory.

In all measurements, the choice of the lower energy endpoint is set by the limits of electron identification and prevailing backgrounds. Only the electronic lepton channel is measured, on the basis that the precision of electron measurement is far greater than that for muons, with less material involved in the detection system. The electron energy moments measurements are statistically limited, but not the partial branching fractions.

II. DATA SAMPLE, DETECTOR AND SIMULATION

The data used in this analysis were collected with the Belle detector at the KEKB [16] asymmetric energy e^+e^- collider. The Belle [17] detector is a large-solid-angle magnetic spectrometer that consists of a three-layer silicon vertex detector (SVD), a 50-layer central drift chamber (CDC), an array of aerogel threshold Čerenkov counters (ACC), a barrel-like arrangement of time-of-flight scintillation counters (TOF), and an electromagnetic calorimeter comprised of CsI(Tl) crystals (ECL) located inside a superconducting solenoid coil that provides a 1.5 T magnetic field. An iron flux-return located outside of the coil is instrumented to detect K_L^0 mesons and to identify muons (KLM).

The present results are based on a 140 fb^{-1} data sample collected at the $\Upsilon(4S)$ resonance (on-resonance), which contains 1.52×10^8 $B\bar{B}$ pairs. An additional 15 fb^{-1} data sample taken at 60 MeV below the $\Upsilon(4S)$ resonance (off-resonance) is used to perform subtraction of background arising from the continuum $e^+e^- \to q\bar{q}$ process. Events are selected by fully reconstructing one of the B mesons, produced in pairs from $\Upsilon(4S)$ decays.

We use Monte Carlo (MC) techniques to simulate the production and decay of B mesons, and the detector response. The simulated sample of generic $B\bar{B}$ events is equivalent to 3 times the on-resonance integrated luminosity. In addition we use a simulated sample of $B \to X_u\ell\nu$ events equivalent to 25 times the expected rate in data. Simulated events are generated with the EVTGEN event generator [18] and processed through the Belle detector simulation based on GEANT [19].

For the simulation of $B \to X_c e\nu$ decays, we have chosen a variety of models. For $B \to De\nu$ and $B \to D^*e\nu$ decays we use parametrizations [20–22] of the form factors, based on heavy quark effective theory (HQET). Decays to pseudoscalar mesons are described by a single form factor $F_D(w)/F_D(1) = 1 - \rho_D^2(w - 1)$, where the variable w is the scalar product of the B and D meson four-vector velocities. We use the world average value of the slope parameter $\rho_D^2 = 1.17 \pm 0.18$ [23]. The rate for $B \to D^*e\nu$ can be described by three amplitudes, which depend on three parameters denoted ρ^2, R_1 and R_2. We adopt the world average value, $\rho^2 = 1.19 \pm 0.06$ [23] and the most recently measured values for $R_1 = 1.396 \pm 0.075$ and $R_2 = 0.885 \pm 0.047$ [24]. The branching fractions of the D and D^* components are based on values reported in the Review of Particle Physics [25].

Details of the various decays to higher mass D^{**} resonances are less well known. The $D^{**}e\nu$ component includes both narrow orbitally excited charmed mesons and broad resonances. The existence of both the broad and narrow resonant states is well established [26], however, only the narrow state semileptonic branching fractions have been measured [27], with limits placed on the broad state branching fractions. Decay shape characteristics of these states in semileptonic B decays have not been measured and must be estimated from theory predictions. We use the model by Leibovich *et al.* [28] (LLSW). Differential decay rates are predicted for various resonant $D^{**}e\nu$ decays, using limits from measurements to resonant states (semileptonic [27] and hadronic [26]), as well as the full rate to $D^{(*)}\pi e\nu$ states [29], and full inclusive rates [25]. These limits enable an estimate of the $1/m_Q$ corrections to the currently used ISGW2 decay models [30]. The uncertainty on the measured $D^{**}e\nu$ resonances, in conjunction with the theoretical estimates provide bounds on the differential decay rates (and branching fractions) of the $D^{**}e\nu$ contributions. We have adopted a prescription by Goity and Roberts [31] for the nonresonant $B \to D^{(*)}\pi e\nu$ decay shapes.

The MC sample used to model background $b \to u$ events is a hybrid mix of inclusive and exclusive contributions. The exclusive channels π, ρ and ω decays are produced with the SLPOLE model [18]. Other resonant semileptonic decays (charged $a_{0,1,2}$, b_1 for neutral B and neutral η, η', $a_{0,1,2}$, b_1, $f_{0,1,2}$ for charged B) are simulated with the ISGW2 model [30]. Contributions from the in-

clusive part of the mix are implemented with the shape function parametrization (defined in Ref. [32]). The inclusive branching fraction is set to the world average value, $\mathcal{B}(B \to X_u \ell \nu) = (2.16 \pm 0.33) \times 10^{-3}$ [23].

III. EVENT SELECTION

We first identify hadronic events based on charged track multiplicity and total visible energy, suppressing backgrounds from QED, $e^+ e^- \to \tau^+ \tau^-$, and beam-gas events. The selection procedure is described in detail elsewhere [33]. We then fully reconstruct one B meson in one of several hadronic modes to determine its charge, flavor, and momentum, referred to as the "tagside" B (B_{tag}). The B_{tag} candidates are reconstructed in the decay modes $B^+ \to \bar{D}^{(*)0} \pi^+$, $\bar{D}^{(*)0} \rho^+$, $\bar{D}^{(*)0} a_1^+$ and $B^0 \to D^{(*)-} \pi^+$, $D^{(*)-} \rho^+$, $D^{(*)-} a_1^+$, yielding a high purity B meson sample. The following subdecay modes of the charmed meson are reconstructed:

   (i) $\bar{D}^{*0} \to \bar{D}^0 \pi^0$, $\bar{D}^0 \gamma$,
   (ii) $D^{*-} \to \bar{D}^0 \pi^-$, $D^- \pi^0$,
   (iii) $\bar{D}^0 \to K^+ \pi^-$, $K^+ \pi^- \pi^0$, $K^+ \pi^- \pi^- \pi^+$, $K_S \pi^+ \pi^-$, $K_S^0 \pi^0$ and
   (iv) $D^- \to K^+ \pi^- \pi^+$, $K_S^0 \pi$.

For each selected event, we calculate the beam-energy constrained mass, M_{bc}, and the energy difference, ΔE:

$$M_{\text{bc}} = \sqrt{(E_{\text{beam}}^*)^2 - (p_B^*)^2}, \qquad \Delta E = E_B^* - E_{\text{beam}}^*, \quad (1)$$

where E_{beam}^*, p_B^* and E_B^* are the beam energy, the reconstructed B momentum and the reconstructed B energy in the center of mass frame, respectively. Events with $5.27 \text{ GeV}/c^2 < M_{\text{bc}} < 5.29 \text{ GeV}/c^2$ and $-0.06 \text{ GeV} < \Delta E < 0.08 \text{ GeV}$ are considered for further analysis. In this region the B_{tag} purity is 66% (72%) for B^+ (B^0) tags. The number of B^+ and B^0 candidates (with statistical errors) in the signal region (N_{tag}), after continuum and combinatorial background (due to incorrect reconstruction or tagging of the tagged B) subtraction, is 63185 ± 621 and 39504 ± 392, respectively. Subtraction of these backgrounds is performed with the same method as used for prompt electron events, and is described in detail later.

IV. ELECTRON SELECTION AND ELECTRON MOMENTUM RECONSTRUCTION

A. Identification and selection

We search for electrons produced by semileptonic B decays on the "nontag" side. Electron candidates are required to originate from near the interaction vertex and pass through the barrel region of the detector, corresponding to an angular acceptance of $35° < \theta_{\text{lab}} < 125°$, where θ_{lab} denotes the polar angle of the electron candidate with respect to the direction opposite to the positron beam. We exclude tracks used in the reconstruction of the B_{tag} and

multiple reconstructed tracks generated by low-momentum particles spiralling in the drift chamber.

Electron candidates are selected on the basis of the ratio of the energy detected in the ECL to the track momentum, matching between the positions of the charged track and ECL cluster, the ECL shower shape, the energy loss in the drift chamber and the response of the ACC [17]. In events with multiple identified electrons, only the highest momentum electron is considered as an electron candidate. The electron identification efficiency and the probabilities to misidentify a pion, kaon or proton as an electron have been measured as a function of the laboratory momentum and angles. The average electron identification efficiency and hadron misidentification rate are 97% and 0.7%, respectively, over the full phase space.

B. Bremsstrahlung recovery

Because of the emission of highly energetic photons from electrons, the determination of electron momenta solely from reconstructed track information results in the reconstructed momenta being softer than expected. To alleviate this, the momentum of each electron is determined using additional information from the ECL. Neutral clusters of energy below 1 GeV contained within a cone of 0.05 radians around the electron track direction from the interaction point are added to the electron energy. The radius of the cone around the electron has been chosen to maximize the signal to noise ratio for photons emitted by electrons. The photon energy cut optimizes the electron energy resolution, as over-correction for photon radiation causes a significant bias of the reconstructed momentum.

Photon radiation may be due to either bremsstrahlung radiation in the detector material in front of the ECL, or to QED radiation in the decay process. Simulation of detector bremsstrahlung in the detector material in front of the ECL requires that the description of the material be very precise. The method of summing all radiated photons in proximity to the track decreases the dependence on the accuracy of the material description. Prompt photons due to high order QED corrections are accounted for in the MC with the use of the PHOTOS package [34].

The electron momenta are calculated in the B meson rest frame (p_e^{*B}), exploiting the knowledge of the momentum of the fully reconstructed B. We require $p_e^{*B} \geq 0.4 \text{ GeV}/c$. The stated selection criteria result in an efficiency of 45–65% for selecting $B \to X_c e \nu$ decays, which is dependent on the electron energy.

V. BACKGROUND SUBTRACTION

The reconstructed electron momentum spectrum is contaminated by background processes, which are evaluated and subtracted from the distribution before the extraction of the moments. Contamination of the spectrum is predominantly due to continuum background, combinatorial background, cascade charm decays $b \to c \to q \ell \nu$ (second-

ary), J/ψ, $\psi(2S)$, Dalitz decays, photon conversions, fake electrons and $B \to X_u \ell \nu$ decays. These will be described in turn.

A. Non-$B\bar{B}$ background

The shape of the continuum background is derived from off-resonance data, and is normalized using the off- to on-resonance luminosity ratio and cross section difference. The statistical uncertainty of the continuum normalization factor is determined by the number of detected Bhabha events used for the measurement of the integrated luminosity. There are very few events in the off-resonance data that pass the event and particle selection criteria so we choose to fit an exponential to the off-resonance p_e^{*B} distribution before renormalizing, of the form $f(\vec{a}, p_e^{*B}) = \exp(a_1 + a_2 p_e^{*B})$, where $\vec{a}$ are the set of free parameters in the fit.

B. $B\bar{B}$ background

In the charged B-meson sample, prompt semileptonic decays ($b \to q\ell\nu$) of the "nontag" side B mesons are separated from cascade charm decays ($b \to c \to q\ell\nu$), based on the correlation between the flavor of the tagging B and the electron charge. In neutral B-meson decays, mixing may occur, flipping the correlation. Thus in the neutral B sample we do not require this correlation.

1. Combinatorial

True $B\bar{B}$ events for which reconstruction or flavor assignment of the tagged B meson is not correct are considered background events (which we refer to as combinatorial background). This background has a peaking structure in the signal region of M_{bc}. We derive the shape of this background from generic $B\bar{B}$ MC events, where each particle used in the reconstruction of B_{tag} corresponds directly to what was generated in the simulation. The yield of this background is normalized to the on-resonance data M_{bc} sideband (5.20 GeV/c^2 < M_{bc} < 5.25 GeV/c^2) after

the subtraction of non-$B\bar{B}$ backgrounds. Figure 1 displays the M_{bc} distribution after electron selection cuts, ΔE cuts and continuum subtraction, independently for the B^+ and B^0 electron samples. The contributions from the combinatorial background are overlaid.

2. Subtraction of $B \to X_u e \nu$

The contribution of electrons from the inclusive $b \to u$ transition are subtracted from the electron momentum spectrum. This component of the background is normalized to the number of B^+ and B^0 tags, assuming the world average value for the inclusive charmless semileptonic branching fraction.

3. Fit to the inclusive spectra

All remaining backgrounds arise when the fully reconstructed B is correctly tagged, but the electron candidate either is from a secondary decay or is a misidentified hadron. These background sources are irreducible.

The background from $B \to D^{(*)} \to e$ decays is determined from MC simulation, adjusting the contribution of these events to the world average $B \to D$ anything and semileptonic D branching fractions [25]. Contributions from J/ψ and $\psi(2S)$ decays, photon conversions, and Dalitz decays, also determined by MC simulation, are small after our selection cuts. Hadronic B decays additionally contribute via hadron misidentification (i.e. π fakes).

We estimate the overall normalization of these remaining backgrounds by fitting the observed inclusive electron momentum spectrum to the sum of the MC-simulated signal and background contributions, after continuum, combinatorial and $B \to X_u e \nu$ background subtraction. The fit is performed in the range 0.4 GeV/c < p_e^{*B} < 2.4 GeV/c, treating the relative normalization factors of the signal and background as the two free parameters in the fit. The values of the χ^2 per degree of freedom for the fits to B^+ and B^0 decay spectra are 1.3 and 1.1, respectively. Figure 2 shows the electron momentum spectrum with all background contributions overlaid, before corrections due to detector effects and selection efficiencies. Confirmation
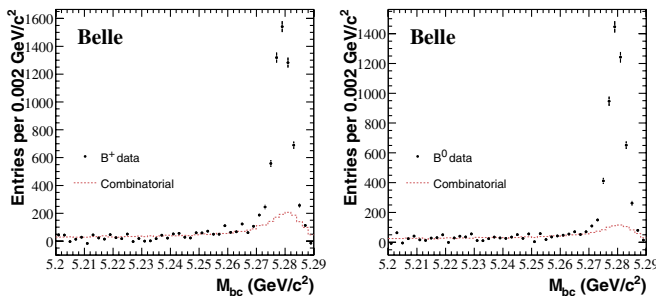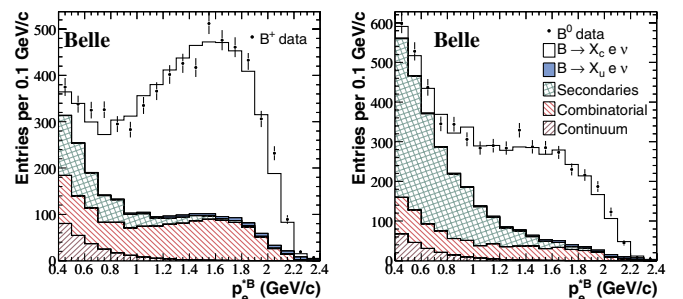

FIG. 1 (color online). The data points represent the beam-energy constrained mass, M_{bc}, after electron selection cuts, ΔE cuts and continuum subtraction for the B^+ electron sample (left), and the B^0 electron sample (right). The histogram represents the peaking combinatorial background determined from MC.

FIG. 2 (color online). Measured electron momentum spectra from B^+ and B^0 decays before background subtraction, overlaid with the various backgrounds and the MC signal. Secondaries also includes hadron fakes. The errors shown are statistical only.

TABLE I. Electron yields for $p_e^{*B} \geq 0.4$ GeV/c. The errors are statistical only.

B candidate	B^+	B^0
On-Resonance Data	6423 ± 80	5403 ± 74
Scaled Off Resonance	249 ± 48	209 ± 39
Combinatorial Background	1244 ± 20	696 ± 13
Secondary (Inc. Hadron Fakes)	555 ± 11	1843 ± 22
$B \rightarrow X_u e \nu$	74 ± 5	57 ± 6
Background Subtracted	4300 ± 96	2597 ± 87

of the agreement between the data and the signal and background MC can be seen in these plots, and has been furthermore checked in M_{bc} and ΔE sideband regions, where the signal contribution is less dominant. The electron yields after particle selection cuts and subtraction of backgrounds are given in Table I.

VI. THE ELECTRON ENERGY SPECTRUM

A. Unfolding

To measure the moments of the electron energy spectrum, we need to determine the true electron energy spectrum in the B meson rest frame, E_e^{*B}. In this analysis we assume the electron to be massless, imposing $E_e^{*B} = p_e^{*B}$. The measured electron energy spectrum is distorted by various detector effects. Hence, the true electron energy spectrum is extracted by performing an unfolding procedure based on the Singular Value Decomposition (SVD) algorithm [35]. The reliability of the unfolding procedure is dependent on the agreement between data and MC simulation, both for the physics models and the detector response. Studies of MC show that there are no biases due to the SVD unfolding algorithm.

The unfolded spectrum is corrected for QED radiative effects using the PHOTOS algorithm [34], as the OPE does
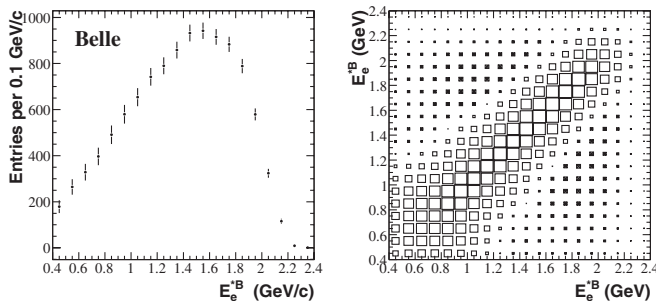

FIG. 3. Unfolded electron energy distribution in the B meson rest frame(left), combining contributions from B^0 and B^+ decays, and corrected for QED radiative effects, detector and selection efficiencies. The errors shown are statistical. On the right is the corresponding unfolded electron energy distribution covariance matrix, where the filled boxes represent negative elements. (These plots are shown for illustrative purposes only.)

not have $\mathcal{O}(\alpha)$ QED corrections. The unfolded electron energy spectrum and the bin-to-bin statistical covariance matrix calculated with the unfolding algorithm are shown in Fig. 3 (for illustrative purposes only, as the full error analysis is performed on a moment measurement basis).

B. Moments and partial branching fractions

We measure the first four central moments of the electron energy spectrum with nine electron energy threshold values ($E_{cut} = 0.4, 0.6, 0.8, 1.0, 1.2, 1.4, 1.6, 1.8, 2.0$ GeV in the B rest frame) combining the spectra from B^+ and B^0 semileptonic decays. The first moment is defined to be $M_1^I = \langle E_e^{*B} \rangle_{E_e^{*B} > E_{cut}^I}$ and subsequent central moments are calculated about the first moment, $M_n^I = \langle (E_e^{*B} - M_1^I)^n \rangle_{E_e^{*B} > E_{cut}^I}$, where I is the index for the electron energy threshold and $n = 2, 3, 4$. The statistical uncertainty of each moment is calculated as:

$$\sigma_{stat}^2(M_n^I) = \frac{\Sigma_{ij}(E_{e,i}^{*B} - M_1^I)^n X_{ij}(E_{e,j}^{*B} - M_1^I)^n}{(\Sigma_i x_i')^2} \Bigg|_{E_{e,i(j)}^{*B} > E_{cut}^I},$$

(2)

where x' is the unfolded spectrum in the B rest frame, corrected for the bin-to-bin detection efficiencies, X is the covariance matrix, and $E_{e,i(j)}^{*B}$ is the central value of bin $i(j)$ in the B rest frame.

In addition, we measure the partial branching fractions, combining the spectra from B^+ and B^0 semileptonic decays, and independently measuring the B^+ and B^0 partial branching fractions at the previous lower electron energy threshold of 0.6 GeV [15] and a new lower electron energy threshold of 0.4 GeV. The expression for the partial branching fraction and its statistical error is calculated as:

$$\Delta \mathcal{B}^I = \frac{\Sigma_i(x_i'')}{N_{tag}} \Bigg|_{E_{e,i(j)}^{*B} > E_{cut}^I},$$

$$\sigma_{stat,\Delta\mathcal{B}^I}^2 = \left[\left(\frac{\sqrt{\Sigma_{ij} X_{ij}''}}{N_{tag}} \right)^2 + \left(\frac{\Sigma_i(x_i'') \Delta N_{tag}}{N_{tag}^2} \right)^2 \right]_{E_{e,i(j)}^{*B} > E_{cut}^I},$$

(3)

where N_{tag} is the number of tagged B events, and x'' and X'' denote the full efficiency corrected unfolded spectrum and covariance matrix, respectively.

VII. SYSTEMATIC ERRORS

The contributions to the systematic error for each moment and electron energy threshold are summarized in Tables II, III, IV, V, and VI for all moments and partial branching fraction measurements. The total systematic error is obtained by adding each contribution in quadrature. The principal systematic errors originate from the event selection, electron identification, background estimation and signal model dependence.

TABLE II. Breakdown of the systematic errors for the first moment, M_1, for $B \to X_c e\nu$ in the B meson rest frame for nine values of the electron energy threshold E_{cut}.

E_{cut} [GeV]	M_1 [MeV]								
	0.4	0.6	0.8	1.0	1.2	1.4	1.6	1.8	2.0
Electron Detection	0.81	0.77	0.42	0.16	0.05	0.09	0.02	0.02	0.01
$(D^{(*)}e\nu)$ form factors	0.59	0.62	0.61	0.47	0.33	0.75	0.80	0.99	1.20
$\mathcal{B}(D^{(*)}e\nu)$	0.22	0.17	0.11	0.11	0.09	0.09	0.05	0.10	0.07
$(D^{**}e\nu)$ form factors	1.71	1.03	0.47	0.10	0.09	0.08	0.10	0.12	0.02
$\mathcal{B}(D^{(*)}_{non-res}\pi e\nu/D^{**}e\nu)$	1.15	1.37	1.50	0.96	0.66	0.38	0.28	0.30	0.16
Continuum	0.02	0.00	0.02	0.02	0.01	0.01	0.01	0.00	0.00
M_{bc}	1.14	0.72	0.24	0.02	0.03	0.05	0.08	0.05	0.04
$X_u e\nu$	0.79	0.78	0.77	0.75	0.72	0.67	0.56	0.36	0.14
Hadron Fakes	0.65	0.56	0.42	0.24	0.11	0.04	0.01	0.00	0.00
$B \to D^{(*)} \to e$	0.91	0.79	0.60	0.39	0.21	0.10	0.04	0.01	0.00
Secondaries	0.82	0.68	0.49	0.27	0.12	0.04	0.01	0.00	0.00
Unfolding	0.02	0.23	0.28	0.24	0.04	0.06	0.10	0.33	0.04
Total Systematics	3.02	2.55	2.13	1.45	1.08	1.10	1.03	1.16	1.23

A. Detector related uncertainties

The selection efficiency for $B \to X_c e\nu$ decays is determined by MC simulation. There are three major factors that determine the detection efficiency: the track reconstruction of the electron, the electron identification, and event selection.

The uncertainty in the tracking efficiency has been studied in detail in Ref. [15], which is estimated to be a 1% effect on the overall efficiency. The electron identification efficiency is determined with a radiative Bhabha sample with dependence on the electron energy in the laboratory frame, and the angle subtended by the electron in the detector. The effect of the difference between the $B\bar{B}$ event environment and the simpler radiative Bhabha environment (two charged tracks and one shower) is studied with embedded samples and a correction for this bias is performed on the measured spectrum. This bias decreases at higher electron momenta. The systematic error associated to the difference between MC and data tracking resolution is negligible. We assess the impact of these uncertainties on the observed spectrum for both the signal and the background. Improvements have been made in the understanding of this systematic error with respect to similar previous measurements [15].

TABLE III. Breakdown of the systematic errors for the second moment, M_2, for $B \to X_c e\nu$ in the B meson rest frame for nine values of the electron energy threshold E_{cut}.

E_{cut} [GeV]	M_2 [10^{-3} GeV^2]								
	0.4	0.6	0.8	1.0	1.2	1.4	1.6	1.8	2.0
Electron Detection	0.27	0.31	0.16	0.08	0.03	0.01	0.00	0.00	0.00
$(D^{(*)}e\nu)$ form factors	0.55	0.38	0.34	0.27	0.31	0.21	0.19	0.18	0.19
$\mathcal{B}(D^{(*)}e\nu)$	0.12	0.11	0.02	0.04	0.02	0.02	0.02	0.01	0.02
$(D^{**}e\nu)$ form factors	0.87	0.44	0.18	0.06	0.04	0.02	0.02	0.00	0.00
$\mathcal{B}(D^{(*)}_{non-res}\pi e\nu/D^{**}e\nu)$	0.75	0.66	0.23	0.08	0.09	0.04	0.04	0.01	0.01
Continuum	0.00	0.00	0.00	0.00	0.00	0.00	0.00	0.00	0.00
M_{bc}	0.38	0.24	0.07	0.03	0.01	0.01	0.01	0.00	0.00
$X_u e\nu$	0.27	0.25	0.23	0.19	0.15	0.11	0.06	0.03	0.01
Hadron Fakes	0.15	0.11	0.06	0.03	0.01	0.00	0.00	0.00	0.00
$B \to D^{(*)} \to e$	0.19	0.13	0.07	0.03	0.01	0.00	0.00	0.00	0.00
Secondaries	0.20	0.14	0.07	0.03	0.01	0.00	0.00	0.00	0.00
Unfolding	0.56	0.34	0.04	0.02	0.00	0.02	0.07	0.01	0.00
Total Systematics	1.53	1.08	0.55	0.36	0.36	0.34	0.22	0.18	0.19

TABLE IV. Breakdown of the systematic errors for the third moment, M_3, for $B \rightarrow X_c e\nu$ in the B meson rest frame for nine values of the electron energy threshold E_{cut}.

	M_3 [10^{-3} GeV^3]								
E_{cut}[GeV]	0.4	0.6	0.8	1.0	1.2	1.4	1.6	1.8	2.0
Electron Detection	0.15	0.06	0.03	0.01	0.01	0.00	0.00	0.00	0.00
$(D^{(*)}e\nu)$ form factors	0.26	0.17	0.15	0.13	0.09	0.06	0.05	0.04	0.03
$\mathcal{B}(D^{(*)}e\nu)$	0.01	0.03	0.02	0.01	0.00	0.01	0.00	0.00	0.00
$(D^{**}e\nu)$ form factors	0.07	0.03	0.03	0.01	0.00	0.00	0.00	0.00	0.00
$\mathcal{B}(D^{(*)}_{\text{non-res}}\pi e\nu/D^{**}e\nu)$	0.46	0.35	0.18	0.10	0.04	0.02	0.01	0.00	0.00
Continuum	0.00	0.00	0.00	0.00	0.00	0.00	0.00	0.00	0.00
M_{bc}	0.16	0.12	0.08	0.02	0.02	0.00	0.00	0.00	0.00
$X_u e\nu$	0.07	0.06	0.04	0.03	0.02	0.01	0.00	0.00	0.00
Hadron Fakes	0.10	0.08	0.06	0.03	0.01	0.00	0.00	0.00	0.00
$B \rightarrow D^{(*)} \rightarrow e$	0.10	0.09	0.07	0.03	0.01	0.00	0.00	0.00	0.00
Secondaries	0.08	0.07	0.05	0.02	0.01	0.00	0.00	0.00	0.00
Unfolding	0.28	0.20	0.13	0.10	0.03	0.03	0.01	0.00	0.00
Total Systematics	0.66	0.49	0.30	0.20	0.11	0.07	0.05	0.04	0.03

B. Uncertainties in the signal spectrum

The branching fractions for exclusive semileptonic $B \rightarrow X_c e\nu$ are not precisely known, particularly D^{**} contributions. For this reason, we introduce a scale factor in the background fits to adjust the overall normalization of the prompt contribution. In addition, we adjust the individual branching fractions of each exclusive $B \rightarrow X_c e\nu$ decay mode. To test the sensitivity to the shape of the signal contributions, we have varied the form factors for the prompt decay types $D^*e\nu$, and $De\nu$, and changed the model input parameters which describe the differential decay rates of the resonant $D^{**}e\nu$ decays.

For $B \rightarrow D^{(*)}e\nu$ decays we use HQET parametrizations of the form factors. To study the impact of the uncertainties in the measured form factors, we reweight the MC-simulated spectrum for a given decay mode to reproduce the change in the spectrum due to the variations of the form-factor parameters. From the observed changes in the signal yield and shape, as a function of the choice of the form-factor parameters for $D^*e\nu$ decays, we assess the systematic error on the moments by varying the form-factor parameters, ρ^2 [23], R_1 and R_2 by 1 standard deviation [24]. For $De\nu$ decays, we rely on measurements of ρ_D^2. Similarly, we estimate the impact of the uncertainty in ρ_D^2

TABLE V. Breakdown of the systematic errors for the fourth moment, M_4, for $B \rightarrow X_c e\nu$ in the B meson rest frame for nine values of the electron energy threshold E_{cut}.

	M_4 [10^{-3} GeV^4]								
E_{cut}[GeV]	0.4	0.6	0.8	1.0	1.2	1.4	1.6	1.8	2.0
Electron Detection	0.042	0.119	0.052	0.021	0.005	0.001	0.000	0.000	0.000
$(D^{(*)}e\nu)$ form factors	0.466	0.250	0.186	0.123	0.098	0.052	0.031	0.016	0.007
$\mathcal{B}(D^{(*)}e\nu)$	0.067	0.067	0.015	0.015	0.008	0.004	0.003	0.001	0.001
$(D^{**}e\nu)$ form factors	0.519	0.206	0.066	0.017	0.009	0.003	0.001	0.000	0.000
$\mathcal{B}(D^{(*)}_{\text{non-res}}\pi e\nu/D^{**}e\nu)$	0.483	0.345	0.088	0.026	0.018	0.005	0.003	0.001	0.000
Continuum	0.001	0.001	0.000	0.000	0.000	0.000	0.000	0.000	0.000
M_{bc}	0.160	0.090	0.021	0.012	0.004	0.002	0.000	0.000	0.000
$X_u e\nu$	0.181	0.138	0.094	0.056	0.030	0.012	0.004	0.001	0.000
Hadron Fakes	0.049	0.036	0.019	0.007	0.002	0.000	0.000	0.000	0.000
$B \rightarrow D^{(*)} \rightarrow e$	0.079	0.046	0.022	0.008	0.002	0.000	0.000	0.000	0.000
Secondaries	0.085	0.050	0.023	0.008	0.002	0.000	0.000	0.000	0.000
Unfolding	0.270	0.157	0.027	0.002	0.014	0.008	0.004	0.000	0.000
Total Systematics	0.935	0.548	0.247	0.142	0.106	0.055	0.032	0.017	0.007

TABLE VI. Breakdown of the systematic errors for the partial branching fractions, $\Delta \mathcal{B}$ for $B \to X_c e \nu$ in the B meson rest frame for nine values of the electron energy threshold E_{cut}.

E_{cut}[GeV]	$\Delta \mathcal{B}$ [10^{-2}]								
	0.4	0.6	0.8	1.0	1.2	1.4	1.6	1.8	2.0
Electron Detection	0.17	0.17	0.15	0.14	0.12	0.10	0.06	0.03	0.01
$(D^{(*)}e\nu)$ form factors	0.01	0.01	0.01	0.01	0.01	0.01	0.01	0.01	0.01
$\mathcal{B}(D^{(*)}e\nu)$	0.05	0.05	0.04	0.04	0.03	0.02	0.02	0.01	0.00
$(D^{**}e\nu)$ form factors	0.05	0.04	0.03	0.02	0.01	0.01	0.01	0.00	0.00
$\mathcal{B}(D^{(*)}_{\text{non-res}}\pi e\nu/D^{**}e\nu)$	0.09	0.09	0.09	0.07	0.05	0.03	0.02	0.01	0.00
Continuum	0.04	0.04	0.03	0.03	0.03	0.02	0.01	0.01	0.00
M_{bc}	0.04	0.03	0.02	0.01	0.00	0.00	0.00	0.00	0.00
$X_u e\nu$	0.03	0.03	0.03	0.03	0.02	0.02	0.02	0.01	0.01
Hadron Fakes	0.02	0.01	0.01	0.01	0.00	0.00	0.00	0.00	0.00
$B \to D^{(*)} \to e$	0.02	0.02	0.02	0.01	0.01	0.00	0.00	0.00	0.00
Secondaries	0.02	0.02	0.01	0.01	0.00	0.00	0.00	0.00	0.00
Unfolding	0.02	0.01	0.00	0.00	0.00	0.00	0.00	0.00	0.00
Total Systematics	0.22	0.21	0.19	0.17	0.14	0.11	0.07	0.04	0.03

[23] by comparing the change on the moments, corresponding to variations of ρ_D^2 by 1 standard deviation.

To assess the impact of the poorly known branching fractions and differential decay rates for various resonant $D^{**}e\nu$ decay we take into account limits from measurements to resonant and nonresonant $D^{(*)}\pi e\nu$ states, and full inclusive rates [25–27,29]. We determine the systematic variation on the moments by varying the LLSW [28] model parameters for the differential decay rates, within their allowed ranges imposed by measurement and theory arguments. Predictions for $D^{**}e\nu$ shapes and branching fractions are assumed to be fully correlated as they rely on the same set of parameters. We use half of the shift between the LLSW model parameter bounds, as an estimate of the systematic error due to the uncertainty in B to D^{**} decays. The branching fraction for nonresonant $D^{(*)}\pi e\nu$ decay modes are assumed to be uncorrelated with the D^{**} decays, and the systematic variation on the moments is estimated as half of the shift between the bounds on the branching fraction.

C. Background subtraction

Systematic errors in the subtraction of the non-$B\bar{B}$ background are dominated by the uncertainty in the relative normalization of the on- and off-resonance data. The error arises from the uncertainty of the measured luminosities, which is estimated to be a 1% error on the continuum electron yield.

The shapes of the $B\bar{B}$ backgrounds are derived from MC simulations. The uncertainty due to mistagging in the B^0 and B^+ samples is estimated by varying the lower bound on the M_{bc} signal region, corresponding to a 10% variation in the ratio of good tags to incorrect tags in the signal region.

The uncertainty due to the $b \to u$ subtraction, which occurs before unfolding, is evaluated by varying the total inclusive charmless branching fraction by 1 standard deviation [23].

The uncertainty due to secondary, cascade $B \to D \to e$ decays is assessed by varying the branching fractions of semileptonic D decays, and $B \to D$ *anything* by 1 standard deviation [25]. This contribution is significant in the neutral B sample as there is no cut on the correlation between the flavor of the tagging B and the electron charge. For background from hadronic B decays, the uncertainty is primarily due to the uncertainty in the hadron misidentification. The uncertainty associated to the magnitude of the hadron fake contribution is determined from a comparison of the fake rates measured with $K_S^0 \to \pi^+ \pi^-$ decays in real data and in the MC simulation.

The systematic uncertainty due to the overall fit for the secondaries to the data is estimated by varying the lower p_e^{*B} bound of the fit region, and the number of bins used in the fit.

D. Unfolding and radiative corrections

For the uncertainties related to the unfolding procedure, we vary the effective rank parameter by one in the SVD algorithm. Corrections for QED radiation in the decay process are simulated using PHOTOS. The simulation includes multiple-photon emission from the electron, and interference effects. The accuracy of this simulation has been compared to analytical calculations performed at $O(\alpha)$ [36]. Based on this comparison, the uncertainty of

the PHOTOS correction leads to a negligible contribution to the overall systematic error.

VII. CORRELATIONS

All measurements performed on the $B \to X_c e \nu$ electron energy spectrum are correlated, with both overlapping data samples, and common systematics. The following de-

scribes the procedure for calculating the covariance and correlations between measurements of the partial inclusive branching fractions and the moments at varying threshold energies.

The statistical covariance matrix of two correlated moment measurements, $\mathrm{cov}_{\mathrm{stat}}[M_k^I, M_l^J]$, is simply a general case of the error calculation:

$$\mathrm{cov}_{\mathrm{stat}}[M_k^I, M_l^J] = \frac{\Sigma_{ij}(E_{e,i}^{*B} - M_1^I)^k X_{ij}(E_{e,j}^{*B} - M_1^J)^l}{\Sigma_i(x_i')\Sigma_j(x_j')}\Bigg|_{E_{e,i}^{*B} > E_{\mathrm{cut}}^I, E_{e,j}^{*B} > E_{\mathrm{cut}}^J}, \tag{4}$$

where k and l are the order of the moments and I and J are indices for the threshold energies. For covariance matrices including the partial branching fractions (zeroth moments), $\Delta \mathcal{B}_{I(J)}$, the factors $1/\Sigma_{i(j)}(x_{i(j)}')$ in Eq. (4) are not present.

The systematic covariance matrix is calculated assuming correlations between individual systematic variations to be positive ($\rho = 1$), negative ($\rho = -1$) or zero ($\rho = 0$), thus;

TABLE VII. Measured moments, M_1, M_2, M_3, M_4 and the partial branching fraction for $B \to X_c e \nu$ in the B meson rest frame for nine values of the threshold electron energy E_{cut}. The first error is statistical, and the second error is the systematic.

| E_{cut} [GeV]	M_1 [MeV]	M_2 [10^{-3} GeV^2]	M_3 [10^{-3} GeV^3]	M_4 [10^{-3} GeV^4]	$\Delta\mathcal{B}$ [10^{-2}]
0.4	$1393.92 \pm 6.73 \pm 3.02$	$168.77 \pm 3.68 \pm 1.53$	$-21.04 \pm 1.93 \pm 0.66$	$64.153 \pm 1.813 \pm 0.935$	$10.44 \pm 0.19 \pm 0.22$
0.6	$1427.82 \pm 5.82 \pm 2.55$	$146.15 \pm 2.88 \pm 1.08$	$-11.04 \pm 1.35 \pm 0.49$	$45.366 \pm 1.108 \pm 0.548$	$10.07 \pm 0.18 \pm 0.21$
0.8	$1480.04 \pm 4.81 \pm 2.13$	$117.97 \pm 2.05 \pm 0.55$	$-3.45 \pm 0.83 \pm 0.30$	$28.701 \pm 0.585 \pm 0.247$	$9.42 \pm 0.16 \pm 0.19$
1.0	$1547.76 \pm 3.96 \pm 1.45$	$88.17 \pm 1.42 \pm 0.36$	$0.83 \pm 0.49 \pm 0.20$	$15.962 \pm 0.302 \pm 0.142$	$8.41 \pm 0.15 \pm 0.17$
1.2	$1627.79 \pm 3.26 \pm 1.08$	$61.36 \pm 1.02 \pm 0.36$	$2.40 \pm 0.30 \pm 0.11$	$7.876 \pm 0.162 \pm 0.106$	$7.11 \pm 0.13 \pm 0.14$
1.4	$1719.96 \pm 2.58 \pm 1.10$	$38.99 \pm 0.71 \pm 0.24$	$2.33 \pm 0.16 \pm 0.07$	$3.314 \pm 0.080 \pm 0.055$	$5.52 \pm 0.11 \pm 0.11$
1.6	$1826.15 \pm 1.80 \pm 1.03$	$21.75 \pm 0.47 \pm 0.22$	$1.45 \pm 0.08 \pm 0.05$	$1.129 \pm 0.033 \pm 0.032$	$3.71 \pm 0.09 \pm 0.07$
1.8	$1943.18 \pm 0.93 \pm 1.16$	$10.14 \pm 0.28 \pm 0.18$	$0.68 \pm 0.03 \pm 0.04$	$0.283 \pm 0.010 \pm 0.017$	$1.93 \pm 0.06 \pm 0.04$
2.0	$2077.59 \pm 0.21 \pm 1.23$	$3.47 \pm 0.13 \pm 0.19$	$0.19 \pm 0.01 \pm 0.03$	$0.047 \pm 0.002 \pm 0.007$	$0.53 \pm 0.02 \pm 0.02$
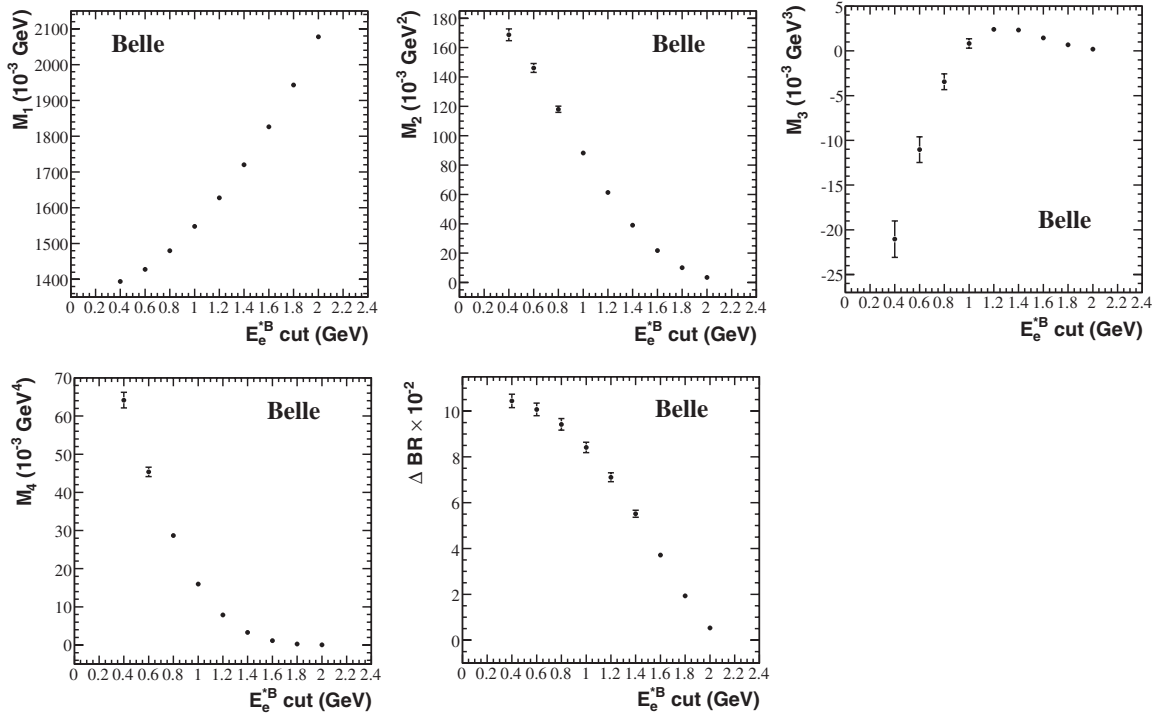
FIG. 4. First, second, third and fourth electron energy moments and partial branching fractions (M_1, M_2, M_3, M_4, $\Delta\mathcal{B}$), as a function of the electron threshold energy E_{cut}. The errors shown are the statistical and systematic errors added in quadrature.

$$\mathrm{cov}_{\mathrm{sys}}[M_k^I, M_l^J] = \rho_{\mathrm{sys}(M_k^I, M_l^J)} \sigma_{\mathrm{sys}, M_k^I} \sigma_{\mathrm{sys}, M_l^J}. \quad (5)$$

summing over all systematic variations.

To obtain the overall covariance matrix, we add the statistical and systematic covariance matrices together. The total correlation between measurements, $\rho_{M_k^I, M_l^J}$, is then derived from the overall covariance matrix and the total errors for each measurement, using a similar expression to Eq. (5).

IX. RESULTS

Table VII provides the B^0 and B^+ weighted average moments as a function of E_{cut}. Figure 4 illustrates these results. The measurement of the first electron energy moment, M_1, at $E_{\mathrm{cut}} = 0.6$ GeV, is $(1427.82 \pm 5.82(\mathrm{stat.}) \pm 2.55(\mathrm{sys.}))$ MeV, which is consistent with, and improves

upon measurements by *BABAR* [12] and CLEO [11]. The independent partial branching fraction measurements of B^+ and B^0 at 0.4 GeV and 0.6 GeV electron energy thresholds are provided with a breakdown of their systematic uncertainties in Table VIII. The results, $\Delta\mathcal{B}(B^+ \to X_c e\nu, E_{\mathrm{cut}} = 0.6\,\mathrm{GeV}) = (10.34 \pm 0.23(\mathrm{stat.}) \pm 0.25(\mathrm{sys.}))\%$ and $\Delta\mathcal{B}(B^0 \to X_c e\nu, E_{\mathrm{cut}} = 0.6\,\mathrm{GeV}) = (9.80 \pm 0.29(\mathrm{stat.}) \pm 0.21(\mathrm{sys.}))\%$, are consistent with our previous measurements [15], with the overall errors improved by approximately 30%. The observed $\Delta\mathcal{B}(B^+ \to X_c e\nu)/\Delta\mathcal{B}(B^0 \to X_c e\nu)$ ratio, at $E_{\mathrm{cut}} = 0.4$ GeV, is $1.07 \pm 0.04(\mathrm{stat.}) \pm 0.03(\mathrm{sys.})$, consistent with the B^+/B^0 lifetime ratio at $\tau_+/\tau_0 = 1.076 \pm 0.008$ [25]. The correlation coefficients for each moment (including the averaged partial branching fractions) and cut combination, are presented in Tables IX, X, XI, XII, XIII, XIV, XV, XVI, XVII, XVIII, XIX, XX, XXI, XXII, and XXIII.

TABLE VIII. Results and breakdown of the systematic errors for the partial branching fractions of charmed semileptonic B decays, independently measured for B^+ and B^0 decays with electron energy threshold values of 0.4 GeV and 0.6 GeV.

E_{cut} [GeV]	$\Delta\mathcal{B}(B^+)$ $[10^{-2}]$		$\Delta\mathcal{B}(B^0)$ $[10^{-2}]$	
	0.4	0.6	0.4	0.6
Electron Detection	0.18	0.17	0.17	0.16
$(D^{(*)}e\nu)$ form factors	0.01	0.01	0.01	0.01
$\mathcal{B}(D^{(*)}e\nu)$	0.08	0.07	0.02	0.02
$(D^{**}e\nu)$ form factors	0.05	0.04	0.04	0.03
$\mathcal{B}(D_{\mathrm{non\text{-}res}}^{(*)}\pi e\nu/D^{**}e\nu)$	0.09	0.09	0.10	0.10
Continuum	0.10	0.09	0.04	0.04
M_{bc}	0.10	0.08	0.04	0.03
$X_u e\nu$	0.04	0.04	0.03	0.03
Hadron fakes	0.02	0.02	0.02	0.02
$B \to D^{(*)} \to e$	0.00	0.00	0.04	0.04
Secondaries	0.08	0.06	0.02	0.02
Unfolding	0.02	0.01	0.06	0.06
$\Delta\mathcal{B}$	10.79	10.34	10.08	9.80
$\pm(\mathrm{stat.})$	0.25	0.23	0.30	0.29
$\pm(\mathrm{sys.})$	0.27	0.25	0.22	0.21

TABLE IX. Correlation coefficients between M_1 measurements, ρ_{M_1, M_1}.

	$M_1^{0.4}$	$M_1^{0.6}$	$M_1^{0.8}$	$M_1^{1.0}$	$M_1^{1.2}$	$M_1^{1.4}$	$M_1^{1.6}$	$M_1^{1.8}$	$M_1^{2.0}$
$M_1^{0.4}$	1.00	0.97	0.86	0.65	0.47	0.33	0.25	0.10	0.05
$M_1^{0.6}$	0.97	1.00	0.94	0.76	0.59	0.42	0.31	0.14	0.13
$M_1^{0.8}$	0.86	0.94	1.00	0.92	0.77	0.56	0.41	0.16	0.15
$M_1^{1.0}$	0.65	0.76	0.92	1.00	0.92	0.73	0.55	0.26	0.11
$M_1^{1.2}$	0.47	0.59	0.77	0.92	1.00	0.90	0.72	0.40	0.19
$M_1^{1.4}$	0.33	0.42	0.56	0.73	0.90	1.00	0.93	0.67	0.36
$M_1^{1.6}$	0.25	0.31	0.41	0.55	0.72	0.93	1.00	0.83	0.46
$M_1^{1.8}$	0.10	0.14	0.16	0.26	0.40	0.67	0.83	1.00	0.68
$M_1^{2.0}$	0.05	0.13	0.15	0.11	0.19	0.36	0.46	0.68	1.00

TABLE X.   Correlation coefficients between M_1 and M_2 measurements, ρ_{M_1,M_2}.

	$M_2^{0.4}$	$M_2^{0.6}$	$M_2^{0.8}$	$M_2^{1.0}$	$M_2^{1.2}$	$M_2^{1.4}$	$M_2^{1.6}$	$M_2^{1.8}$	$M_2^{2.0}$
$M_1^{0.4}$	-0.51	-0.42	-0.27	0.75	-0.23	0.11	0.17	0.18	0.09
$M_1^{0.6}$	-0.44	-0.37	-0.26	0.67	-0.11	0.17	0.21	0.20	0.11
$M_1^{0.8}$	-0.26	-0.22	-0.18	0.72	0.08	0.24	0.27	0.23	0.12
$M_1^{1.0}$	0.01	0.04	0.03	0.11	0.26	0.39	0.42	0.34	0.05
$M_1^{1.2}$	0.31	0.33	0.30	0.27	0.32	0.47	0.50	0.46	0.20
$M_1^{1.4}$	0.47	0.51	0.53	0.53	0.51	0.56	0.60	0.53	0.25
$M_1^{1.6}$	0.50	0.56	0.59	0.64	0.66	0.69	0.68	0.66	0.40
$M_1^{1.8}$	0.43	0.49	0.57	0.65	0.71	0.80	0.80	0.75	0.56
$M_1^{2.0}$	0.28	0.34	0.37	0.43	0.48	0.64	0.68	0.80	0.84

TABLE XI.   Correlation coefficients between M_1 and M_3 measurements, ρ_{M_1,M_3}.

	$M_3^{0.4}$	$M_3^{0.6}$	$M_3^{0.8}$	$M_3^{1.0}$	$M_3^{1.2}$	$M_3^{1.4}$	$M_3^{1.6}$	$M_3^{1.8}$	$M_3^{2.0}$
$M_1^{0.4}$	0.77	0.71	0.57	0.35	0.24	0.27	0.24	0.30	0.10
$M_1^{0.6}$	0.76	0.74	0.64	0.47	0.34	0.34	0.28	0.33	0.10
$M_1^{0.8}$	0.72	0.73	0.72	0.66	0.54	0.47	0.40	0.44	0.18
$M_1^{1.0}$	0.55	0.59	0.70	0.77	0.74	0.65	0.58	0.40	0.09
$M_1^{1.2}$	0.36	0.44	0.60	0.76	0.84	0.83	0.73	0.53	0.30
$M_1^{1.4}$	0.29	0.36	0.48	0.63	0.78	0.87	0.83	0.71	0.45
$M_1^{1.6}$	0.23	0.30	0.41	0.51	0.62	0.80	0.84	0.72	0.63
$M_1^{1.8}$	0.17	0.26	0.37	0.42	0.48	0.66	0.73	0.69	0.80
$M_1^{2.0}$	0.04	0.11	0.20	0.21	0.23	0.39	0.45	0.57	0.92

TABLE XII.   Correlation coefficients between M_1 and M_4 measurements, ρ_{M_1,M_4}.

	$M_4^{0.4}$	$M_4^{0.6}$	$M_4^{0.8}$	$M_4^{1.0}$	$M_4^{1.2}$	$M_4^{1.4}$	$M_4^{1.6}$	$M_4^{1.8}$	$M_4^{2.0}$
$M_1^{0.4}$	-0.58	-0.49	-0.34	0.42	-0.53	0.05	0.17	0.24	0.10
$M_1^{0.6}$	-0.50	-0.43	-0.30	0.61	-0.13	0.19	0.26	0.32	0.20
$M_1^{0.8}$	-0.29	-0.23	-0.18	-0.15	0.19	0.34	0.37	0.44	0.25
$M_1^{1.0}$	0.06	0.07	0.05	0.19	0.38	0.53	0.59	0.37	0.07
$M_1^{1.2}$	0.30	0.34	0.33	0.34	0.43	0.63	0.68	0.52	0.44
$M_1^{1.4}$	0.41	0.45	0.50	0.52	0.56	0.70	0.76	0.62	0.55
$M_1^{1.6}$	0.37	0.44	0.46	0.53	0.57	0.70	0.73	0.74	0.72
$M_1^{1.8}$	0.26	0.31	0.39	0.43	0.47	0.62	0.66	0.70	0.85
$M_1^{2.0}$	0.16	0.21	0.23	0.25	0.27	0.43	0.48	0.60	0.93

TABLE XIII.   Correlation coefficients between M_1 and $\Delta\mathcal{B}$ measurements, $\rho_{M_1,\Delta\mathcal{B}}$.

	$\Delta\mathcal{B}^{0.4}$	$\Delta\mathcal{B}^{0.6}$	$\Delta\mathcal{B}^{0.8}$	$\Delta\mathcal{B}^{1.0}$	$\Delta\mathcal{B}^{1.2}$	$\Delta\mathcal{B}^{1.4}$	$\Delta\mathcal{B}^{1.6}$	$\Delta\mathcal{B}^{1.8}$	$\Delta\mathcal{B}^{2.0}$
$M_1^{0.4}$	-0.36	-0.36	-0.31	-0.17	-0.08	-0.04	-0.03	-0.08	-0.04
$M_1^{0.6}$	-0.30	-0.31	-0.28	-0.17	-0.10	-0.05	-0.02	-0.10	-0.05
$M_1^{0.8}$	-0.14	-0.18	-0.21	-0.16	-0.11	-0.06	-0.02	-0.08	-0.02
$M_1^{1.0}$	-0.09	-0.12	-0.13	-0.07	-0.08	-0.06	-0.04	-0.04	-0.02
$M_1^{1.2}$	0.10	0.08	0.07	0.07	0.01	-0.07	-0.18	-0.02	0.00
$M_1^{1.4}$	0.26	0.26	0.27	0.28	0.22	0.09	0.00	-0.09	0.03
$M_1^{1.6}$	0.44	0.47	0.47	0.50	0.47	0.38	0.24	0.09	0.07
$M_1^{1.8}$	0.42	0.47	0.55	0.64	0.69	0.63	0.57	0.41	0.17
$M_1^{2.0}$	0.32	0.36	0.43	0.55	0.63	0.62	0.63	0.59	0.31

TABLE XIV. Correlation coefficients between M_2 measurements, ρ_{M_2,M_2}.

	$M_2^{0.4}$	$M_2^{0.6}$	$M_2^{0.8}$	$M_2^{1.0}$	$M_2^{1.2}$	$M_2^{1.4}$	$M_2^{1.6}$	$M_2^{1.8}$	$M_2^{2.0}$
$M_2^{0.4}$	1.00	0.95	0.83	0.58	0.41	0.38	0.37	0.35	0.26
$M_2^{0.6}$	0.95	1.00	0.91	0.69	0.52	0.44	0.41	0.40	0.29
$M_2^{0.8}$	0.83	0.91	1.00	0.90	0.73	0.61	0.57	0.52	0.35
$M_2^{1.0}$	0.58	0.69	0.90	1.00	0.92	0.79	0.73	0.68	0.48
$M_2^{1.2}$	0.41	0.52	0.73	0.92	1.00	0.94	0.85	0.80	0.58
$M_2^{1.4}$	0.38	0.44	0.61	0.79	0.94	1.00	0.95	0.87	0.63
$M_2^{1.6}$	0.37	0.41	0.57	0.73	0.85	0.95	1.00	0.95	0.74
$M_2^{1.8}$	0.35	0.40	0.52	0.68	0.80	0.87	0.95	1.00	0.88
$M_2^{2.0}$	0.26	0.29	0.35	0.48	0.58	0.63	0.74	0.88	1.00

TABLE XV. Correlation coefficients between M_2 and M_3 measurements, ρ_{M_2,M_3}.

	$M_3^{0.4}$	$M_3^{0.6}$	$M_3^{0.8}$	$M_3^{1.0}$	$M_3^{1.2}$	$M_3^{1.4}$	$M_3^{1.6}$	$M_3^{1.8}$	$M_3^{2.0}$
$M_2^{0.4}$	-0.55	-0.49	-0.29	-0.51	0.26	0.39	0.40	0.37	0.28
$M_2^{0.6}$	-0.52	-0.47	-0.26	-0.09	0.30	0.44	0.43	0.45	0.32
$M_2^{0.8}$	-0.29	-0.25	-0.13	0.11	0.40	0.55	0.60	0.58	0.43
$M_2^{1.0}$	0.49	0.64	-0.07	0.22	0.44	0.62	0.71	0.71	0.55
$M_2^{1.2}$	0.03	0.13	0.27	0.38	0.49	0.65	0.81	0.80	0.65
$M_2^{1.4}$	0.18	0.28	0.39	0.51	0.59	0.67	0.81	0.86	0.76
$M_2^{1.6}$	0.17	0.28	0.41	0.54	0.64	0.70	0.81	0.89	0.89
$M_2^{1.8}$	0.09	0.18	0.33	0.46	0.57	0.63	0.74	0.84	0.96
$M_2^{2.0}$	-0.03	0.05	0.16	0.24	0.32	0.34	0.47	0.67	0.92

TABLE XVI. Correlation coefficients between M_2 and M_4 measurements, ρ_{M_2,M_4}.

	$M_4^{0.4}$	$M_4^{0.6}$	$M_4^{0.8}$	$M_4^{1.0}$	$M_4^{1.2}$	$M_4^{1.4}$	$M_4^{1.6}$	$M_4^{1.8}$	$M_4^{2.0}$
$M_2^{0.4}$	0.98	0.93	0.74	0.45	0.29	0.26	0.26	0.27	0.28
$M_2^{0.6}$	0.94	0.95	0.83	0.58	0.42	0.36	0.33	0.36	0.32
$M_2^{0.8}$	0.84	0.89	0.97	0.84	0.69	0.59	0.59	0.55	0.45
$M_2^{1.0}$	0.59	0.67	0.86	0.95	0.90	0.81	0.80	0.78	0.67
$M_2^{1.2}$	0.41	0.49	0.67	0.83	0.93	0.90	0.90	0.87	0.78
$M_2^{1.4}$	0.37	0.42	0.55	0.72	0.86	0.91	0.95	0.93	0.85
$M_2^{1.6}$	0.32	0.35	0.46	0.61	0.73	0.80	0.90	0.94	0.94
$M_2^{1.8}$	0.26	0.28	0.34	0.47	0.58	0.63	0.74	0.86	0.98
$M_2^{2.0}$	0.17	0.16	0.19	0.28	0.36	0.39	0.52	0.71	0.94

TABLE XVII. Correlation coefficients between M_2 and $\Delta\mathcal{B}$ measurements, $\rho_{M_2,\Delta\mathcal{B}}$.

	$\Delta\mathcal{B}^{0.4}$	$\Delta\mathcal{B}^{0.6}$	$\Delta\mathcal{B}^{0.8}$	$\Delta\mathcal{B}^{1.0}$	$\Delta\mathcal{B}^{1.2}$	$\Delta\mathcal{B}^{1.4}$	$\Delta\mathcal{B}^{1.6}$	$\Delta\mathcal{B}^{1.8}$	$\Delta\mathcal{B}^{2.0}$
$M_2^{0.4}$	0.54	0.57	0.58	0.53	0.41	0.35	0.26	0.20	0.12
$M_2^{0.6}$	0.47	0.52	0.56	0.54	0.44	0.37	0.26	0.20	0.12
$M_2^{0.8}$	0.49	0.54	0.59	0.59	0.52	0.41	0.35	0.24	0.16
$M_2^{1.0}$	0.29	0.33	0.43	0.51	0.53	0.47	0.40	0.26	0.17
$M_2^{1.2}$	0.29	0.35	0.42	0.51	0.56	0.52	0.47	0.32	0.19
$M_2^{1.4}$	0.31	0.37	0.41	0.48	0.55	0.58	0.57	0.41	0.26
$M_2^{1.6}$	0.27	0.31	0.39	0.49	0.56	0.62	0.66	0.54	0.34
$M_2^{1.8}$	0.23	0.29	0.42	0.56	0.63	0.69	0.74	0.70	0.48
$M_2^{2.0}$	0.25	0.33	0.42	0.56	0.61	0.72	0.79	0.71	0.60

TABLE XVIII. Correlation coefficients between M_3 measurements, ρ_{M_3,M_3}.

	$M_3^{0.4}$	$M_3^{0.6}$	$M_3^{0.8}$	$M_3^{1.0}$	$M_3^{1.2}$	$M_3^{1.4}$	$M_3^{1.6}$	$M_3^{1.8}$	$M_3^{2.0}$
$M_3^{0.4}$	1.00	0.97	0.86	0.57	0.39	0.35	0.29	0.14	0.02
$M_3^{0.6}$	0.97	1.00	0.94	0.71	0.52	0.46	0.41	0.23	0.10
$M_3^{0.8}$	0.86	0.94	1.00	0.90	0.73	0.63	0.57	0.39	0.21
$M_3^{1.0}$	0.57	0.71	0.90	1.00	0.93	0.81	0.72	0.51	0.30
$M_3^{1.2}$	0.39	0.52	0.73	0.93	1.00	0.94	0.85	0.63	0.38
$M_3^{1.4}$	0.35	0.46	0.63	0.81	0.94	1.00	0.95	0.75	0.49
$M_3^{1.6}$	0.29	0.41	0.57	0.72	0.85	0.95	1.00	0.89	0.67
$M_3^{1.8}$	0.14	0.23	0.39	0.51	0.63	0.75	0.89	1.00	0.89
$M_3^{2.0}$	0.02	0.10	0.21	0.30	0.38	0.49	0.67	0.89	1.00

TABLE XIX. Correlation coefficients between M_3 and M_4 measurements, ρ_{M_3,M_4}.

	$M_4^{0.4}$	$M_4^{0.6}$	$M_4^{0.8}$	$M_4^{1.0}$	$M_4^{1.2}$	$M_4^{1.4}$	$M_4^{1.6}$	$M_4^{1.8}$	$M_4^{2.0}$
$M_3^{0.4}$	-0.65	-0.57	-0.35	0.35	-0.18	0.08	0.07	-0.04	-0.13
$M_3^{0.6}$	-0.55	-0.49	-0.28	0.70	0.08	0.26	0.26	0.16	0.05
$M_3^{0.8}$	-0.30	-0.27	-0.09	0.14	0.37	0.49	0.53	0.42	0.27
$M_3^{1.0}$	0.04	0.11	0.21	0.35	0.54	0.68	0.73	0.63	0.43
$M_3^{1.2}$	0.31	0.35	0.46	0.56	0.65	0.77	0.85	0.76	0.55
$M_3^{1.4}$	0.38	0.44	0.54	0.69	0.76	0.83	0.90	0.84	0.61
$M_3^{1.6}$	0.34	0.39	0.52	0.68	0.77	0.84	0.94	0.93	0.78
$M_3^{1.8}$	0.27	0.30	0.40	0.51	0.62	0.72	0.87	0.98	0.93
$M_3^{2.0}$	0.16	0.17	0.25	0.34	0.42	0.53	0.71	0.92	0.99

TABLE XX. Correlation coefficients between M_3 and $\Delta\mathcal{B}$ measurements, $\rho_{M_3,\Delta\mathcal{B}}$.

	$\Delta\mathcal{B}^{0.4}$	$\Delta\mathcal{B}^{0.6}$	$\Delta\mathcal{B}^{0.8}$	$\Delta\mathcal{B}^{1.0}$	$\Delta\mathcal{B}^{1.2}$	$\Delta\mathcal{B}^{1.4}$	$\Delta\mathcal{B}^{1.6}$	$\Delta\mathcal{B}^{1.8}$	$\Delta\mathcal{B}^{2.0}$
$M_3^{0.4}$	-0.14	-0.13	-0.10	0.00	0.09	-0.08	0.03	0.06	0.00
$M_3^{0.6}$	-0.06	-0.06	-0.05	0.01	0.08	0.01	0.05	0.08	0.01
$M_3^{0.8}$	0.08	0.06	0.02	0.02	0.06	0.05	0.08	0.10	0.05
$M_3^{1.0}$	-0.02	0.02	0.06	0.09	0.06	0.07	0.10	0.10	0.06
$M_3^{1.2}$	0.25	0.25	0.25	0.21	0.14	0.10	0.13	0.13	0.09
$M_3^{1.4}$	0.23	0.29	0.32	0.34	0.28	0.18	0.17	0.14	0.11
$M_3^{1.6}$	0.28	0.35	0.42	0.49	0.47	0.38	0.32	0.23	0.14
$M_3^{1.8}$	0.32	0.37	0.47	0.55	0.61	0.59	0.57	0.38	0.21
$M_3^{2.0}$	0.30	0.36	0.46	0.56	0.65	0.66	0.72	0.46	0.31

TABLE XXI. Correlation coefficients between M_4 measurements, ρ_{M_4,M_4}.

	$M_4^{0.4}$	$M_4^{0.6}$	$M_4^{0.8}$	$M_4^{1.0}$	$M_4^{1.2}$	$M_4^{1.4}$	$M_4^{1.6}$	$M_4^{1.8}$	$M_4^{2.0}$
$M_4^{0.4}$	1.00	0.97	0.78	0.51	0.36	0.31	0.29	0.28	0.23
$M_4^{0.6}$	0.97	1.00	0.86	0.62	0.46	0.39	0.36	0.31	0.23
$M_4^{0.8}$	0.78	0.86	1.00	0.87	0.70	0.61	0.55	0.43	0.30
$M_4^{1.0}$	0.51	0.62	0.87	1.00	0.92	0.84	0.78	0.65	0.47
$M_4^{1.2}$	0.36	0.46	0.70	0.92	1.00	0.96	0.90	0.77	0.59
$M_4^{1.4}$	0.31	0.39	0.61	0.84	0.96	1.00	0.96	0.84	0.65
$M_4^{1.6}$	0.29	0.36	0.55	0.78	0.90	0.96	1.00	0.94	0.81
$M_4^{1.8}$	0.28	0.31	0.43	0.65	0.77	0.84	0.94	1.00	0.96
$M_4^{2.0}$	0.23	0.23	0.30	0.47	0.59	0.65	0.81	0.96	1.00

TABLE XXII.   Correlation coefficients between M_4 and $\Delta\mathcal{B}$ measurements, $\rho_{M_4,\Delta\mathcal{B}}$.

	$\Delta\mathcal{B}^{0.4}$	$\Delta\mathcal{B}^{0.6}$	$\Delta\mathcal{B}^{0.8}$	$\Delta\mathcal{B}^{1.0}$	$\Delta\mathcal{B}^{1.2}$	$\Delta\mathcal{B}^{1.4}$	$\Delta\mathcal{B}^{1.6}$	$\Delta\mathcal{B}^{1.8}$	$\Delta\mathcal{B}^{2.0}$
$M_4^{0.4}$	0.44	0.50	0.51	0.44	0.29	0.22	0.16	0.09	0.07
$M_4^{0.6}$	0.37	0.44	0.49	0.45	0.31	0.23	0.16	0.09	0.06
$M_4^{0.8}$	0.38	0.46	0.52	0.49	0.39	0.26	0.22	0.14	0.08
$M_4^{1.0}$	0.22	0.24	0.33	0.40	0.39	0.30	0.25	0.14	0.09
$M_4^{1.2}$	0.15	0.16	0.25	0.35	0.40	0.34	0.29	0.17	0.11
$M_4^{1.4}$	0.16	0.26	0.32	0.40	0.42	0.38	0.36	0.21	0.14
$M_4^{1.6}$	0.15	0.20	0.32	0.43	0.46	0.45	0.45	0.29	0.18
$M_4^{1.8}$	0.11	0.20	0.37	0.55	0.58	0.60	0.60	0.40	0.25
$M_4^{2.0}$	0.12	0.21	0.37	0.57	0.61	0.66	0.70	0.44	0.34

TABLE XXIII.   Correlation coefficients between $\Delta\mathcal{B}$ measurements, $\rho_{\Delta\mathcal{B},\Delta\mathcal{B}}$.

	$\Delta\mathcal{B}^{0.4}$	$\Delta\mathcal{B}^{0.6}$	$\Delta\mathcal{B}^{0.8}$	$\Delta\mathcal{B}^{1.0}$	$\Delta\mathcal{B}^{1.2}$	$\Delta\mathcal{B}^{1.4}$	$\Delta\mathcal{B}^{1.6}$	$\Delta\mathcal{B}^{1.8}$	$\Delta\mathcal{B}^{2.0}$
$\Delta\mathcal{B}^{0.4}$	1.00	0.99	0.97	0.93	0.87	0.80	0.71	0.58	0.46
$\Delta\mathcal{B}^{0.6}$	0.99	1.00	0.99	0.95	0.90	0.83	0.74	0.61	0.48
$\Delta\mathcal{B}^{0.8}$	0.97	0.99	1.00	0.98	0.94	0.86	0.77	0.64	0.50
$\Delta\mathcal{B}^{1.0}$	0.93	0.95	0.98	1.00	0.98	0.92	0.83	0.69	0.53
$\Delta\mathcal{B}^{1.2}$	0.87	0.90	0.94	0.98	1.00	0.97	0.89	0.74	0.57
$\Delta\mathcal{B}^{1.4}$	0.80	0.83	0.86	0.92	0.97	1.00	0.96	0.82	0.62
$\Delta\mathcal{B}^{1.6}$	0.71	0.74	0.77	0.83	0.89	0.96	1.00	0.93	0.74
$\Delta\mathcal{B}^{1.8}$	0.58	0.61	0.64	0.69	0.74	0.82	0.93	1.00	0.90
$\Delta\mathcal{B}^{2.0}$	0.46	0.48	0.50	0.53	0.57	0.62	0.74	0.90	1.00

X. SUMMARY

We report a measurement of the electron energy spectrum of the inclusive decay $B \to X_c e\nu$ and its first four moments for threshold energies from 0.4 GeV to 2.0 GeV. In addition we provide the partial branching fraction measurements for the same set of threshold energies, including independent measurements of B^+ and B^0 at threshold energies of 0.4 GeV and 0.6 GeV. The full correlation matrix for this set of measurements has also been evaluated. This set of moments, combined with the moments of the hadronic mass distribution, can serve as input for the determination of HQE parameters and of $|V_{cb}|$.

ACKNOWLEDGMENTS

[1] I. I. Bigi, M. A. Shifman, and N. G. Uraltsev, Annu. Rev. Nucl. Part. Sci. **47**, 591 (1997).

[2] A. V. Manohar and M. B. Wise, Phys. Rev. D **49**, 1310 (1994).

[3] M. Gremm and A. Kapustin, Phys. Rev. D **55**, 6924 (1997).

[4] A. F. Falk, M. Luke, and M. J. Savage, Phys. Rev. D **53**, 2491 (1996); A. F. Falk and M. Luke, Phys. Rev. D **57**, 424 (1998).

[5] P. Gambino and N. G. Uraltsev, Eur. Phys. J. C **34**, 181 (2004); N. G. Uraltsev, Int. J. Mod. Phys. A **20**, 2099 (2005); D. Benson, I. I. Bigi, Th. Mannel, and N. G. Uraltsev, Nucl. Phys. **B665**, 367 (2003).

[6] M. Voloshin and M. Shifman, Sov. J. Nucl. Phys. **45**, 292 (1987); J. Chay, H. Georgi, and B. Grinstein, Phys. Lett. B **247**, 399 (1990); I. I. Bigi, N. G. Uraltsev, and A. I. Vainshtein, Phys. Lett. B **293**, 430 (1992).

[7] K. Wilson, Phys. Rev. **179**, 1499 (1969).

[8] C. W. Bauer, Z. Ligeti, M. Luke, and A. V. Manohar, Phys. Rev. D **67**, 054012 (2003); C. W. Bauer *et al.*, Phys. Rev. D **70**, 094017 (2004).

[9] P. Gambino and N. Uraltsev, Eur. Phys. J. C **34**, 181 (2004).

[10] M. Battaglia *et al.* (DELPHI Collaboration), DELPHI Report No. 2003-028 CONF 648 (unpublished).

[11] A. H. Mahmood *et al.* (CLEO Collaboration), Phys. Rev. D **70**, 032003 (2004).

[12] B. Aubert *et al.* (*BABAR* Collaboration), Phys. Rev. D **69**, 111104 (2004).

[13] K. Abe *et al.* (Belle Collaboration), BELLE, Report No. BELLE-CONF-0558 (unpublished).

[14] Throughout this paper, the inclusion of the charge conjugate mode decay is implied unless otherwise stated.

[15] T. Okabe *et al.* (Belle Collaboration), Phys. Lett. B **614**, 27 (2005).

[16] S. Kurokawa and E. Kikutani, Nucl. Instr. Meth. A **499**, 1 (2003).

[17] K. Hanagaki *et al.* (Belle Collaboration), Nucl. Instr. and Meth. A **485**, 490 (2002).

[18] D. J. Lange, Nucl. Instrum. Methods Phys. Res., Sect. A **462**, 152 (2001).

[19] R. Brun *et al.* (GEANT 3.21), CERN, Report No. DD/EE/ 84-1 (1984) (unpublished).

[20] M. Neubert, Phys. Rep. **245**, 259 (1994).

[21] I. Caprini, L. Lellouch, and M. Neubert, Nucl. Phys. **B530**, 153 (1998).

[22] B. Grinstein and Z. Ligeti, Phys. Lett. B **526**, 345 (2002).

[23] E. Barberio *et al.* (Heavy Flavor Averaging Group), hep-ex/0603003.

[24] B. Aubert *et al.* (*BABAR* Collaboration), Phys. Rev. D **74**, 092004 (2006).

[25] S. Eidelman *et al.*, Phys. Lett. B **592**, 1 (2004).

[26] K. Abe *et al.* (Belle Collaboration), Phys. Rev. Lett. **94**, 221805 (2005); Phys. Rev. D **69**, 112002 (2004).

[27] ALEPH, CDF, DELPHI, L3, OPAL, SLD, hep-ex/ 0112028.

[28] A. K. Leibovich, Z. Ligeti, I. W. Stewart, and M. B. Wise, Phys. Rev. D **57**, 308 (1998).

[29] D. Liventsev, T. Matsumoto *et al.* (Belle Collaboration), Phys. Rev. D **72**, 051109(R) (2005).

[30] D. Scora and N. Isgur, Phys. Rev. D **52**, 2783 (1995); See also N. Isgur *et al.*, Phys. Rev. D **39**, 799 (1989).

[31] J. L. Goity and W. Roberts, Phys. Rev. D **51**, 3459 (1995).

[32] F. De Fazio and N. Neubert, J. High Energy Phys. 06 (1999) 017.

[33] The selection of hadronic events is described in K. Abe *et al.* (Belle Collaboration), Phys. Rev. D **64**, 072001 (2001).

[34] E. Barberio and Z. Was, Comput. Phys. Commun. **79**, 291 (1994).

[35] A. Höcker and V. Kartvelishvili, Nucl. Instr. Meth. A **372**, 469 (1996).

[36] E. Richter-Was, Phys. Lett. B **303**, 163 (1993).